Role of parasitic modes in nonlinear closure via the resolvent feedback loop

Kevin Rosenberg,[*] Sean Symon,[†] and Beverley J. McKeon

Graduate Aerospace Laboratories, California Institute of Technology, Pasadena, California 91125, USA

We use the feedback formulation of McKeon and Sharma [J. Fluid Mech. **658**, 336 (2010)], where the nonlinear term in the Navier-Stokes equations is treated as an intrinsic forcing of the linear resolvent operator, to educe the structure of fluctuations in the range of scales (wave numbers) where linear mechanisms are not active. In this region, the absence of dominant linear mechanisms is reflected in the lack of low-rank characteristics of the resolvent and in the disagreement between the structure of resolvent modes and actual flow features. To demonstrate the procedure, we choose low Reynolds number cylinder flow and the Couette equilibrium solution EQ1, which are representative of very low-rank flows dominated by one linear mechanism. The former is evolving in time, allowing us to compare resolvent modes with dynamic mode decomposition (DMD) modes at the first and second harmonics of the shedding frequency. There is a match between the modes at the first harmonic but not at the second harmonic where there is no separation of the resolvent operator's singular values. We compute the self-interaction of the resolvent mode at the shedding frequency and illustrate its similarity to the nonlinear forcing of the second harmonic. When it is run through the resolvent operator, the "forced" resolvent mode shows better agreement with the DMD mode. A similar phenomenon is observed for the fundamental streamwise wave number of the EQ1 solution and its second harmonic. The importance of parasitic modes, labeled as such since they are driven by the amplified frequencies, is their contribution to the nonlinear forcing of the main amplification mechanisms as shown for the shedding mode, which has subtle discrepancies with its DMD counterpart.

I. INTRODUCTION

The resolvent framework of Ref. [1] can be used for low-order modeling, e.g., Ref. [2], and reconstruction of flows from limited measurements, e.g., Refs. [3,4]. Unlike data-driven methods such as dynamic mode decomposition (DMD), which require snapshots of the fluctuating flow fields, only knowledge of the mean velocity profile is needed to form the resolvent operator which maps nonlinear terms, or forcing, to velocity fluctuations. One of the primary reasons for its success is the tendency for the resolvent operator to be low rank at energetic frequencies. Under such conditions, the optimal mode, which can be obtained via a singular value decomposition (SVD) of the operator, is significantly more amplified than its suboptimal counterparts and hence the flow structure can be approximated without precise knowledge of the nonlinear forcing. Effectively, then, mode structure is obtained by approximating the (action of the) resolvent operator.

Sharma *et al.* [5] and Towne *et al.* [6] have noted a correspondence between resolvent modes, DMD, and spectral proper orthogonal decomposition (SPOD) modes. In particular, Towne *et al.*

---

*Corresponding author: krosenbe@caltech.edu

†Present address: Mechanical Engineering, University of Melbourne, VIC 3010, Australia.

[6] noted that resolvent modes are equivalent to SPOD modes when the nonlinear forcing is uncorrelated in space and time. When the nonlinear forcing is not white noise, resolvent modes deviate from their data-driven counterparts and this is particularly evident at frequencies where the amplification of the optimal mode is not sufficiently higher than the suboptimal modes.

The objective here is to take advantage of the feedback loop described in Refs. [1,7] and determine under what conditions mode shapes can be obtained by the action of the full resolvent on nonlinear forcing computed from resolvent modes, i.e., when it is appropriate to approximate the forcing rather than the resolvent, and how well these modes compare from data-driven counterparts. In this respect, this Rapid Communication will share similarities to weakly nonlinear analyses [8,9] in the sense of considering a limited set of finite-amplitude perturbations and their interactions. However, while weakly nonlinear analyses typically consider the neutral stability of a base flow and expansions in the vicinity of a critical Reynolds number, here we will consider the neutral stability of a mean flow and make no restriction on the Reynolds number range. The flows analyzed herein are cylinder flow and the EQ1 equilibrium solution of Couette flow. Both flows exhibit strong amplification at a single frequency/spatial wave number which is linked to the neutral stability of the temporal mean profile in the case of the cylinder [10] and the streamwise-averaged mean in the case of EQ1 [11]. Reference [12] leveraged this property to develop a self-consistent model for the cylinder where the Reynolds stresses are approximated by the most amplified mode whose amplitude is adjusted until the flow is neutrally stable. In a similar vein, the choice of EQ1 is motivated by previous work analyzing the emergence of streamwise-constant streaks, the scale interactions which give rise to them, and their connections to the self-sustaining process of turbulent shear flows [11,13,14].

II. APPROACH

We consider the incompressible Navier-Stokes equations (NSEs) and decompose the velocity field into a mean component $\overline{\boldsymbol{u}}$ (which is different from the base, laminar flow in each case) and fluctuating component $\boldsymbol{u}'$. In the case of the cylinder, we use a temporal mean with $\overline{\boldsymbol{u}} = [\overline{u}(x, y), \overline{v}(x, y), 0]^T$ and for EQ1 we use a temporal and streamwise-averaged mean with $\overline{\boldsymbol{u}} = [\overline{u}(y, z), \overline{v}(y, z), \overline{w}(y, z)]^T$. While the base/equilibrium states of the flows studied herein are linearly unstable, the operators associated with the corresponding mean flows are not (additional analysis would be required if they were, e.g., Ref. [15]). The resulting equations for the fluctuations are

$$\partial_t \boldsymbol{u}' + \overline{\boldsymbol{u}} \cdot \nabla \boldsymbol{u}' + \boldsymbol{u}' \cdot \nabla \overline{\boldsymbol{u}} + \nabla p' - \mathrm{Re}^{-1} \nabla^2 \boldsymbol{u}' = -\boldsymbol{u}' \cdot \nabla \boldsymbol{u}' + \overline{\boldsymbol{u}' \cdot \nabla \boldsymbol{u}'}, \quad \nabla \cdot \boldsymbol{u}' = \boldsymbol{0}. \tag{1}$$

Following Ref. [1], we define $\boldsymbol{f}' = -\boldsymbol{u}' \cdot \nabla \boldsymbol{u}' + \overline{\boldsymbol{u}' \cdot \nabla \boldsymbol{u}'}$ and treat $\boldsymbol{f}'$ as an unknown forcing. Upon Fourier transforming in the appropriate directions, we can recast Eq. (1) as

$$\hat{\boldsymbol{u}} = \boldsymbol{C}(i\omega \boldsymbol{I} - \boldsymbol{L})^{-1} \boldsymbol{B} \hat{\boldsymbol{f}} = \mathcal{H}(\mathbf{k}) \hat{\boldsymbol{f}}, \tag{2}$$

where $\mathcal{H}(\mathbf{k})$ is the resolvent operator for a particular wave number/frequency vector $\boldsymbol{k}$, $\boldsymbol{L}$ is the linear Navier-Stokes operator associated with the mean, and $\boldsymbol{B}, \boldsymbol{C}$ are operators which define the inputs and outputs; a complete mathematical definition of these operators for these flows is found in Refs. [2,4]. It should be noted for the cylinder flow that $\boldsymbol{k}$ is simply defined by the temporal frequency ω and in the case of EQ1 by the streamwise wave number k_x (and temporal frequency $\omega = 0$, as it is an equilibrium solution). Subsequently, we will analyze the resolvent operators $\mathcal{H}(\omega)$ and $\mathcal{H}(k_x)$ for the two flows, respectively. For generality and to facilitate comparisons between the flows going forward, we will maintain the notation $\mathcal{H}(\mathbf{k})$.

The resolvent operator relies on the mean velocity profile $\overline{\boldsymbol{u}}$ as an input and acts as a transfer function from nonlinearity $\hat{\boldsymbol{f}}(\mathbf{k})$ to velocity fluctuations $\hat{\boldsymbol{u}}(\mathbf{k})$ in Fourier space. A singular value decomposition (SVD) of the resolvent operator,

$$\mathcal{H}(\mathbf{k}) = \sum_p \hat{\boldsymbol{\psi}}_p(\mathbf{k}) \sigma_p(\mathbf{k}) \hat{\boldsymbol{\phi}}_p^*(\mathbf{k}), \tag{3}$$

leads to optimal sets of orthonormal singular response and forcing modes, or $\hat{\boldsymbol{\psi}}_p(\mathbf{k})$ and $\hat{\boldsymbol{\phi}}_p^*(\mathbf{k})$, respectively. The modes are ranked by the forcing-to-response gain $\sigma_p(\mathbf{k})$ under the L_2 norm. When the first singular value is much larger than the second one, i.e., $\sigma_1(\mathbf{k}) \gg \sigma_2(\mathbf{k})$, the velocity response may be approximated as

$$\hat{\boldsymbol{u}}(\mathbf{k}) \approx \hat{\boldsymbol{\psi}}_1(\mathbf{k})\sigma_1(\mathbf{k})\chi_1(\mathbf{k}) = \hat{\boldsymbol{\psi}}_1(\mathbf{k})\sigma_1(\mathbf{k})\langle\hat{\boldsymbol{\phi}}_1(\mathbf{k}), \hat{\boldsymbol{f}}(\mathbf{k})\rangle, \tag{4}$$

where the angle brackets denote the projection of $\hat{\boldsymbol{f}}(\mathbf{k})$ onto $\hat{\boldsymbol{\phi}}_1(\mathbf{k})$. In cases where the singular values are not sufficiently separated and/or the forcing is highly structured, Eq. (4) will not accurately reproduce the velocity fluctuations at a given $\mathbf{k}$.

One course of action is to consider suboptimal resolvent modes ($p > 1$) and project the nonlinear forcing $\hat{\boldsymbol{f}}(\mathbf{k})$ onto the resolvent forcing modes to determine the complex weights χ_p associated with each resolvent response mode. Here, we approximate the structure of the fluctuations when the resolvent operator is not low rank by considering the feedback loop introduced by McKeon $et\ al.$ [7], where the nonlinearity is formed by triadic interactions of the velocity modes, i.e.,

$$\hat{\boldsymbol{f}}(\mathbf{k}_3) = \sum_{\mathbf{k}_1+\mathbf{k}_2=\mathbf{k}_3} -\hat{\boldsymbol{u}}(\mathbf{k}_1) \cdot \boldsymbol{\nabla}\hat{\boldsymbol{u}}(\mathbf{k}_2). \tag{5}$$

The associated nonlinear forcing, consequently, is given by triadically consistent resolvent response modes obtained from the previous singular value decompositions,

$$\hat{\boldsymbol{f}}(\mathbf{k}_3) = \sum_{\mathbf{k}_1+\mathbf{k}_2=\mathbf{k}_3} \sum_a \sum_b -\sigma_a(\mathbf{k}_1)\sigma_b(\mathbf{k}_2)\chi_a(\mathbf{k}_1)\chi_b(\mathbf{k}_2)[\hat{\boldsymbol{\psi}}_a(\mathbf{k}_1) \cdot \boldsymbol{\nabla}\hat{\boldsymbol{\psi}}_b(\mathbf{k}_2)]. \tag{6}$$

All terms on the right-hand side of Eq. (6) can be determined by approximation of the resolvent, with the exception of χ_a and χ_b, which may be obtained only under special circumstances, which we investigate here. In such cases, the forcing from Eq. (6) can then be used to obtain better approximations of the velocity fluctuations for the non-low-rank case.

We compare the mode shapes arising from a rank-one approximation of the resolvent operator with those from an approximation of the forcing for two flows. Both have a strong physical mechanism underlying a dominant coherent structure in a narrow band of scales even though energetic activity is not limited to that band.

A direct numerical simulation (DNS) of two-dimensional cylinder flow is performed in FREEFEM++ [16] using the same mesh, boundary conditions, and discretizations as those in Symon $et\ al.$ [17] at $\mathrm{Re} = UD/\nu = 100$, based on cylinder diameter D, inlet velocity U, and kinematic viscosity ν. The time step is $\Delta t = 0.02$ and the mean is obtained after time averaging over 25 vortex shedding cycles once the flow achieves a steady limit cycle. The linear operators needed for resolvent analysis are formed in FREEFEM++ around the two-dimensional mean flow, and resolvent modes are computed using the procedure outlined in Sipp and Marquet [18]. The DNS snapshots are analyzed using DMD, e.g., Refs. [19,20], to isolate the true structure of the flow at individual frequencies.

The Couette equilibrium solution EQ1 [21,22] is considered under the same domain and discretization as outlined in Ref. [21] with a Reynolds number of $\mathrm{Re} = u^\dagger h/\nu = 1000$, where $u^\dagger$ is half the relative velocity of the moving walls and h is the channel half height. The discrete spatial operators needed to form the resolvent utilize Chebyshev and Fouier differentiation matrices in the wall-normal and spanwise directions, respectively [23].

III. APPROXIMATION OF CYLINDER FLOW AND EXACT COHERENT STATE

Let us denote $\boldsymbol{k}_h$ as the frequency/wave number of the first energetic harmonic for these two flows, i.e., the shedding frequency ω_s and the fundamental streamwise wave number k_{x_f}, respectively. Symon $et\ al.$ [17] showed that low-rank behavior for cylinder flow at $\mathrm{Re} = 100$ is limited to a bandwidth of frequencies in the vicinity of $\boldsymbol{k}_h$. The singular values for $\boldsymbol{k}_h$ are plotted in

Fig. 1(a), which shows $\sigma_1(\boldsymbol{k}_h)$ is two orders of magnitude larger than the rest. While progress can be made with this assumption, the forcing is, in fact, structured and influences the streamwise decay of the resolvent modes. This can be seen in Figs. 1(b) and 1(c), which compare the streamwise component of the resolvent and DMD modes. The overall agreement is good although the mode shapes begin to diverge around $x = 5$.

Similar observations can be made for EQ1. Figure 1(j) indicates very low-rank behavior for $\boldsymbol{k}_h$ and, just as for the cylinder case, the resolvent accurately predicts the mode shape as seen in Figs. 1(k) and 1(l) where the u component of the first resolvent mode is compared to the true solution.

When the resolvent is not low rank, such as at $\boldsymbol{k} = 2\boldsymbol{k}_h$, as seen in Figs. 1(d) and 1(m), respectively, the leading mode from a SVD is unlikely to predict the structure of the velocity fluctuations. Consequently, there is no agreement between the resolvent and DMD modes, which are plotted in Figs. 1(e) and 1(f), respectively, for the cylinder. The unusual shape of the resolvent mode shares similarities to the case of a backward facing step [24]. The resolvent mode and true velocity fluctuations for EQ1 in Figs. 1(n) and 1(o), respectively, also disagree.

In both cases, there is no linear mechanism active at $2\boldsymbol{k}_h$. The analysis of Ref. [25] can be extended to argue which scale interactions are needed in Eq. (6) to recover $\hat{\boldsymbol{f}}(2\boldsymbol{k}_h)$ (note also the similarities with weakly nonlinear analysis of flow near a critical Reynolds number, subject to the differences identified in the Introduction). The linearized NSEs are rewritten as

$$iq\boldsymbol{k}_h\hat{\boldsymbol{u}}(q\boldsymbol{k}_h) = \boldsymbol{L}\hat{\boldsymbol{u}}(q\boldsymbol{k}_h) + \mathcal{N}(q\boldsymbol{k}_h), \tag{7}$$

$$\mathcal{N}(q\boldsymbol{k}_h) = \sum_{r \neq 0, q} \mathcal{N}(\hat{\boldsymbol{u}}(r\boldsymbol{k}_h), \hat{\boldsymbol{u}}(q - r)\boldsymbol{k}_h). \tag{8}$$

For $\|\hat{\boldsymbol{u}}(q\boldsymbol{k}_h)\| \sim \epsilon^{|q|}$, $\epsilon \ll 1$, as it must be for large singular values [Figs. 1(a) and 1(j)], and considering $q = 2$,

$$\underbrace{2i\boldsymbol{k}_h\hat{\boldsymbol{u}}(2\boldsymbol{k}_h)}_{O(\epsilon^2)} = \underbrace{\boldsymbol{L}\hat{\boldsymbol{u}}(2\boldsymbol{k}_h)}_{O(\epsilon^2)} + \underbrace{\mathcal{N}(\hat{\boldsymbol{u}}(\boldsymbol{k}_h), \hat{\boldsymbol{u}}(\boldsymbol{k}_h))}_{O(\epsilon^2)} + \underbrace{\mathcal{N}(\hat{\boldsymbol{u}}(3\boldsymbol{k}_h), \hat{\boldsymbol{u}}(-\boldsymbol{k}_h))}_{O(\epsilon^4)} + \underbrace{\mathcal{N}(\hat{\boldsymbol{u}}(-\boldsymbol{k}_h), \hat{\boldsymbol{u}}(3\boldsymbol{k}_h))}_{O(\epsilon^4)} + \cdots. \tag{9}$$

Retaining $O(\epsilon^2)$ terms results in

$$\hat{\boldsymbol{u}}(2\boldsymbol{k}_h) \approx \mathcal{H}(2\boldsymbol{k}_h)\mathcal{N}(\hat{\boldsymbol{u}}(\boldsymbol{k}_h), \hat{\boldsymbol{u}}(\boldsymbol{k}_h)) \approx -\sigma_1^2\chi_1^2\mathcal{H}(2\boldsymbol{k}_h)[\hat{\boldsymbol{\psi}}_1(\boldsymbol{k}_h) \cdot \nabla\hat{\boldsymbol{\psi}}_1(\boldsymbol{k}_h)], \tag{10}$$

where Eq. (4) is used to approximate $\hat{\boldsymbol{u}}(\boldsymbol{k}_h)$. Terms with the subscript 1 are associated with the wave number vector $\boldsymbol{k}_h$.

Approximating the forcing $\hat{\boldsymbol{f}}(2\boldsymbol{k}_h)$ by the self-interaction of $\hat{\boldsymbol{\psi}}_1(\boldsymbol{k}_h)$ leads to a reasonable comparison with the true forcing for both the cylinder [Figs. 1(g) and 1(h)] and EQ1 [Figs. 1(p) and 1(q)]. The modes excited by these forcings, $\hat{\boldsymbol{u}}_f(2\boldsymbol{k}_h) = \mathcal{H}(2\boldsymbol{k}_h)\hat{\boldsymbol{f}}(2\boldsymbol{k}_h)$, show much improved agreement with the true response at $2\boldsymbol{k}_h$ [Figs. 1(i) and 1(r)].

The EQ1 structures in Figs. 1(r) and 1(o) are nearly identical. While there is significant improvement in the mode shape for the cylinder, the agreement between Fig. 1(i) and the DMD mode in Fig. 1(f) is not perfect. The residual discrepancy for the cylinder is likely due to the fact $\hat{\boldsymbol{\psi}}_1(\boldsymbol{k}_h) \neq \hat{\boldsymbol{u}}(\boldsymbol{k}_h)$ and only one triad was considered. Nevertheless, the forced resolvent mode captures the correct symmetries and is much more representative of the fluctuations at $2\boldsymbol{k}_h$.

The mode at $2\boldsymbol{k}_h$ can be considered "parasitic" in that it is driven by the dominant linear mechanism at $\boldsymbol{k}_h$ and emerges from the resolvent operator being forced by the $\boldsymbol{k}_h$ velocity modes. It
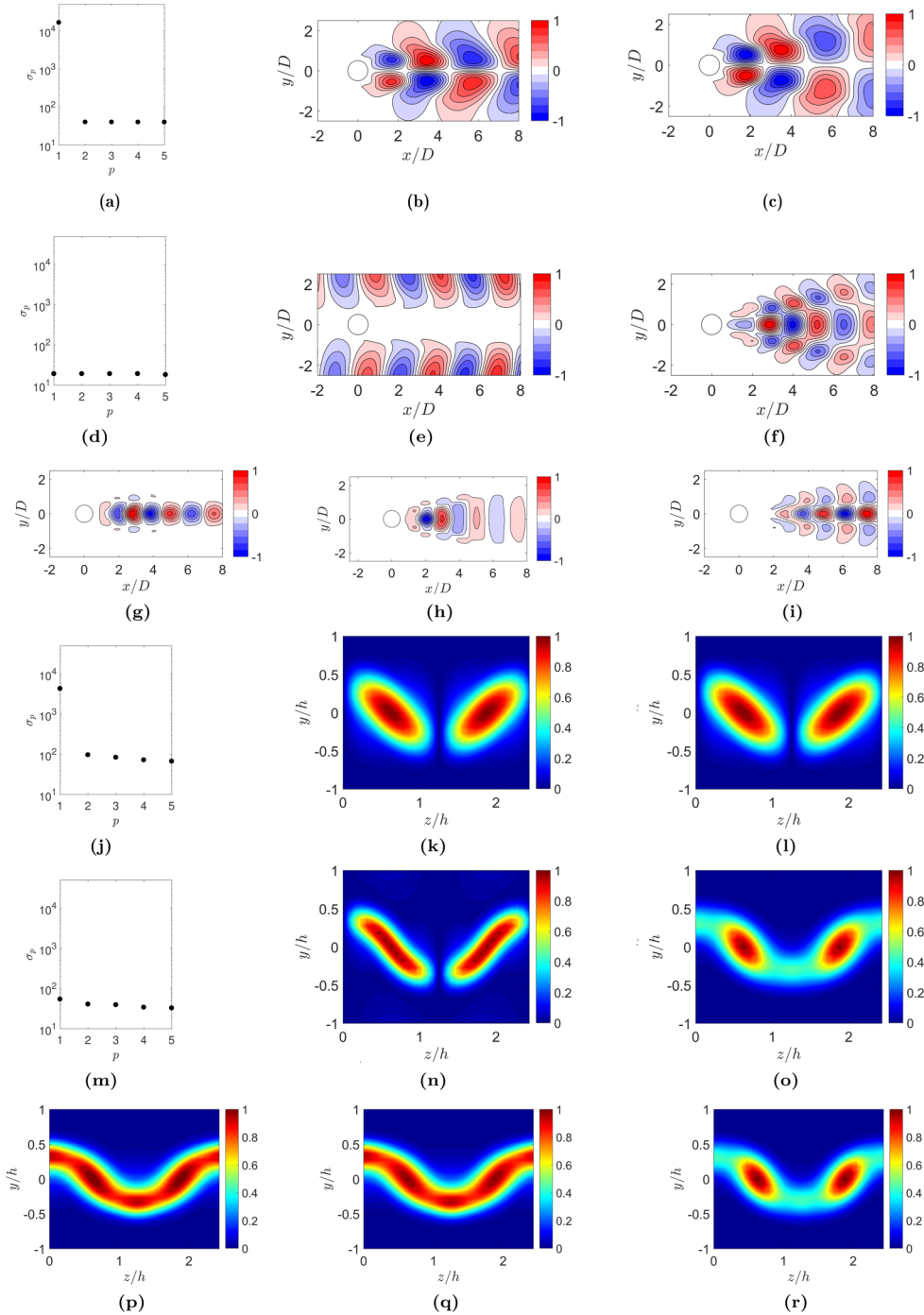
FIG. 1. Rows 1–3: Cylinder results. (a) The leading singular values computed for $\boldsymbol{k}_h$, (b) the u component of the optimal response mode $\hat{\boldsymbol{\psi}}_1(\boldsymbol{k}_h)$, and (c) the corresponding DMD mode. (d) The leading singular values computed for $2\boldsymbol{k}_h$, (e) the u component of the optimal response mode $\hat{\boldsymbol{\psi}}_1(2\boldsymbol{k}_h)$, and (f) the corresponding DMD mode. (g) The self-interaction of $\hat{\boldsymbol{\psi}}_1(\boldsymbol{k}_h)$ compared to the true nonlinear forcing $\hat{\boldsymbol{f}}(2\boldsymbol{k}_h)$ in (h), and (i) the forced resolvent mode (u component) for $2\boldsymbol{k}_h$. Rows 4–6: EQ1 results. As in (a)–(i) but for EQ1.

plays a role in the nonlinear forcing of the $\boldsymbol{k}_h$ mode. Setting $q = 1$ in Eq. (7) results in

$$\underbrace{i\boldsymbol{k}_h\hat{\boldsymbol{u}}(\boldsymbol{k}_h)}_{O(\epsilon)} = \underbrace{\boldsymbol{L}\hat{\boldsymbol{u}}(\boldsymbol{k}_h)}_{O(\epsilon)} + \underbrace{\mathcal{N}(\hat{\boldsymbol{u}}(2\boldsymbol{k}_h), \hat{\boldsymbol{u}}(-\boldsymbol{k}_h))}_{O(\epsilon^3)} + \underbrace{\mathcal{N}(\hat{\boldsymbol{u}}(-\boldsymbol{k}_h), \hat{\boldsymbol{u}}(2\boldsymbol{k}_h))}_{O(\epsilon^3)} + \cdots. \tag{11}$$

It was argued by Turton et $al.$ [25] that the ϵ^3 terms could be neglected, resulting in $\boldsymbol{L}$ containing a marginally stable eigenvalue as discovered by Barkley [10]. Retaining those terms and substituting Eqs. (4) and (10), we can express the forcing as

$$\hat{\boldsymbol{f}}(\boldsymbol{k}_h) = \chi_1|\chi_1|^2\left\{\left[\sigma_1^2\mathcal{H}(2\boldsymbol{k}_h)(\hat{\boldsymbol{\psi}}_1 \cdot \nabla\hat{\boldsymbol{\psi}}_1)\right] \cdot \nabla[\sigma_1\hat{\boldsymbol{\psi}}_1^*] + [\sigma_1\hat{\boldsymbol{\psi}}_1^*] \cdot \nabla\left[\sigma_1^2\mathcal{H}(2\boldsymbol{k}_h)(\hat{\boldsymbol{\psi}}_1 \cdot \nabla\hat{\boldsymbol{\psi}}_1)\right]\right\}$$

$$= \chi_1|\chi_1|^2\hat{\boldsymbol{f}}'(\boldsymbol{k}_h), \tag{12}$$

where notably $\hat{\boldsymbol{f}}'(\boldsymbol{k}_h)$ can be computed from the resolvent with only knowledge of the mean. From Eq. (4) we can solve for the amplitude as

$$|\chi_1| = \left[\frac{1}{\langle\hat{\boldsymbol{\phi}}_1(\boldsymbol{k}_h), \hat{\boldsymbol{f}}'(\boldsymbol{k}_h)\rangle}\right]^{1/2}. \tag{13}$$

From Eq. (11), retaining terms at $O(\epsilon)$ and treating the higher-order terms as an unknown forcing, the resolvent operator can be formulated and used to compute the spatial structure of the mode $\hat{\boldsymbol{\psi}}_1(\boldsymbol{k}_h)$. Consequently, after cascading down the nonlinear interactions, at $O(\epsilon^3)$ an equation can be derived for the corresponding amplitude of the mode, in close analogy to a weakly nonlinear analysis. For EQ1 at Re $= 1000$, this approximation of $|\chi_1|$ has a relative error with respect to the true value computed directly from the solution of less than 1%. As Eq. (12) and the subsequent calculation of $|\chi_1|$ relies on $\hat{\boldsymbol{\psi}}_1(\boldsymbol{k}_h)$ closely approximating the true spatial structure, the agreement in the case of the cylinder is not as good. However, if the DMD modes, which are the true velocity fluctuations at $\boldsymbol{k}_h$ and $2\boldsymbol{k}_h$, are used, they can almost exactly reproduce $\hat{\boldsymbol{f}}(\boldsymbol{k}_h)$ [4], confirming the dominance of this interaction in the full flow. Moreover, if $\mathcal{H}(\boldsymbol{k}_h)$ is driven by this forcing, it results in a forced resolvent mode which very accurately approximates the DMD mode in Fig. 1(c). Thus it is possible to improve predictions from resolvent analysis, even when the operator is low rank, by approximating the nonlinear forcing.

The results for the circular cylinder and EQ1 can be summarized in Fig. 2. A SVD of the resolvent operator at $\boldsymbol{k}_h$ yields a highly amplified mode which interacts nonlinearly with its complex conjugate to produce the Reynolds stresses that sustain the mean profile. It also interacts with itself to produce the forcing at $2\boldsymbol{k}_h$. When $\mathcal{H}(2\boldsymbol{k}_h)$ is driven by this forcing, it results in a "parasitic" mode which nonlinearly interacts with the $-\boldsymbol{k}_h$ mode to produce the structured nonlinear forcing for $\boldsymbol{k}_h$. Thus in the case of the cylinder, where there is a greater mismatch between the resolvent mode and the DMD mode, the original $\boldsymbol{\psi}_1(\boldsymbol{k}_h)$ can be iteratively improved using the feedback loop in Fig. 2.

We hypothesize that the separation of singular values of the resolvent can be used to determine when to approximate the forcing instead of the resolvent for a flow about which there is no a $priori$ information about the dominant physical mechanisms, although further work is required to identify a precise threshold on separation, and this is likely to be flow specific.

IV. SUMMARY

Resolvent analysis was used to identify the linear mechanisms and dominant nonlinear interactions required to provide a self-consistent description of low Reynolds number cylinder flow and the Couette equilibrium solution EQ1. It was demonstrated that the leading resolvent mode, obtained by approximation of the resolvent in a region where it is low rank, is able to correctly capture the spatial structure of the most energetic mode. Considering the relevant scale interactions, i.e., approximating the forcing and leveraging the low-rank nature of the energetic mode, generates improved approximations of the second harmonic, here termed a parasitic mode because of its link to the interactions of the energetic mode and the lack of low-rank behavior of its resolvent.
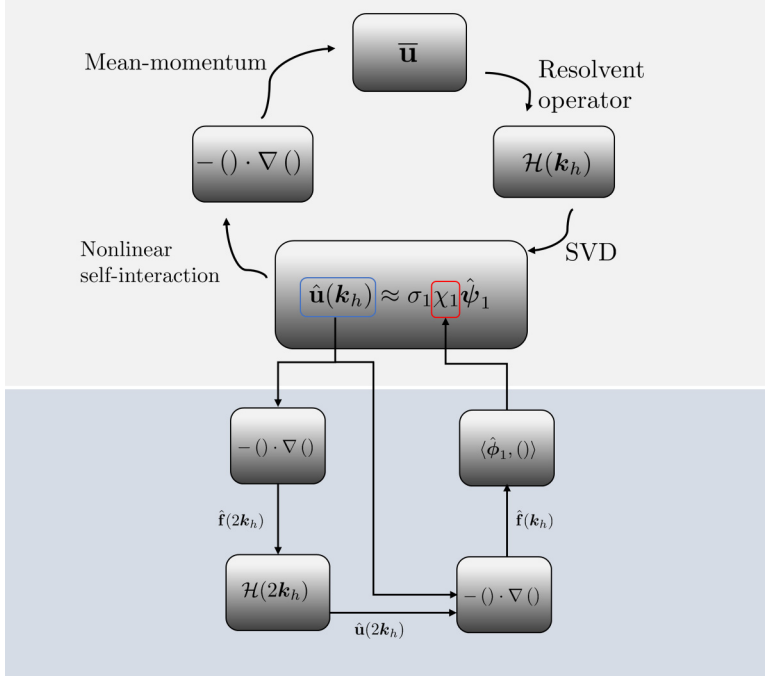
FIG. 2. The top of the schematic illustrates a variation of the self-sustaining process as viewed through the lens of resolvent analysis. The mean profile, fed into the resolvent operator, generates a highly amplified mode (obtained via the SVD) which self-interacts to generate the Reynolds stresses needed to sustain the mean and close the cycle. The saturated amplitude of the mode is obtained by considering the nonlinear interactions which give rise to higher harmonics and their subsequent feedback on the system, as shown in the bottom of the schematic.

These ideas can be consolidated to provide a means to determine the amplitude of the dominant energetic mode, and hence effectively close the system, using knowledge of only the mean profile, in cases where the resolvent is not low rank for all scales. The precise closure and the metric for its success are likely to depend on the specific flow in question, as can be observed in the difference between the cylinder and EQ1 results shown here, because it will rely on the relative importance of the harmonics and other wave numbers through the weights χ_j. However, the interactions sketched in Fig. 2 were shown to give excellent agreement between the computed and actual mode weights for closure of the EQ1 example. It is hypothesized that this framework may also have relevance for flows with multiple linearly dominant energetic modes. We note that data-driven input/output techniques have been utilized to estimate flow features, for instance, in turbulent channel flow [26] and boundary layers [27]. The hope would be to use the resolvent operator to obtain low-dimensional representations of the important linearly amplified structures, which are hypothesized to correspond to identifiable physical mechanisms, and use the notion of parasitic modes to provide an accurate representation of the weakly energetic but nonlinearly relevant scales.

ACKNOWLEDGMENT

[1] B. J. McKeon and A. S. Sharma, A critical-layer framework for turbulent pipe flow, J. Fluid Mech. **658**, 336 (2010).

[2] K. Rosenberg, Resolvent-based modeling of flows in a channel, Ph.D. thesis, California Institute of Technology, 2018.

[3] F. Gómez, H. M. Blackburn, M. Rudman, A. S. Sharma, and B. J. McKeon, A reduced-order model of three-dimensional unsteady flow in a cavity based on the resolvent operator, J. Fluid Mech. **798**, R2 (2016).

[4] S. Symon, Reconstruction and estimation of flows using resolvent analysis and data-assimilation, Ph.D. thesis, California Institute of Technology, 2018.

[5] A. S. Sharma, I. Mezić, and B. J. McKeon, Correspondence between Koopman mode decomposition, resolvent mode decomposition, and invariant solutions of the Navier-Stokes equations, Phys. Rev. Fluids **1**, 032402(R) (2016).

[6] A. Towne, O. T. Schmidt, and T. Colonius, Spectral proper orthogonal decomposition and its relationship to dynamic mode decomposition and resolvent analysis, J. Fluid Mech. **847**, 821 (2018).

[7] B. J. McKeon, A. S. Sharma, and I. Jacobi, Experimental manipulation of wall turbulence: A systems approach, Phys. Fluids **25**, 031301 (2013).

[8] T. Herbert, On perturbation methods in nonlinear stability theory, J. Fluid Mech. **126**, 167 (1983).

[9] D. Sipp and A. Lebedev, Global stability of base and mean flows: A general approach and its applications to cylinder and open cavity flows, J. Fluid Mech. **593**, 333 (2007).

[10] D. Barkley, Linear analysis of the cylinder wake mean flow, Europhys. Lett. **75**, 750 (2006).

[11] P. Hall and S. Sherwin, Streamwise vortices in shear flows: Harbingers of transition and the skeleton of coherent structures, J. Fluid Mech. **661**, 178 (2010).

[12] V. Mantič-Lugo, C. Arratia, and F. Gallaire, Self-Consistent Mean Flow Description of the Nonlinear Saturation of the Vortex Shedding in the Cylinder Wake, Phys. Rev. Lett. **113**, 084501 (2014).

[13] B. F. Farrell and P. J. Ioannou, Dynamics of streamwise rolls and streaks in turbulent wall-bounded shear flow, J. Fluid Mech. **708**, 149 (2012).

[14] F. Waleffe, On a self-sustaining process in shear flows, Phys. Fluids **9**, 883 (1997).

[15] M. R. Jovanović, Modeling, analysis, and control of spatially distributed systems, Ph.D. thesis, University of California at Santa Barbara, 2004.

[16] F. Hecht, New development in FreeFem++, J. Numer. Math. **20**, 251 (2012).

[17] S. Symon, K. Rosenberg, S. T. M. Dawson, and B. J. McKeon, Non-normality and classification of amplification mechanisms in stability and resolvent analysis, Phys. Rev. Fluids **3**, 053902 (2018).

[18] D. Sipp and O. Marquet, Characterization of noise amplifiers with global singular modes: the case of the leading-edge flat-plate boundary layer, Theor. Comput. Fluid Dyn. **27**, 617 (2013).

[19] C. W. Rowley, I., Mezić, S. Bagheri, P. Schlatter, and D. S. Henningson, Spectral analysis of nonlinear flows, J. Fluid Mech. **641**, 115 (2009).

[20] P. J. Schmid, Dynamic mode decomposition of numerical and experimental data, J. Fluid Mech. **656**, 5 (2010).

[21] J. F. Gibson, J. Halcrow, and P. Cvitanović, Equilibrium and travelling-wave solutions of plane Couette flow, J. Fluid Mech. **638**, 243 (2009).

[22] M. Nagata, Three-dimensional finite-amplitude solutions in plane Couette flow: Bifurcation from infinity, J. Fluid Mech. **217**, 519 (1990).

[23] J. A. Weideman and S. C. Reddy, A MATLAB differentiation matrix suite, ACM Trans. Math. Softw. **26**, 465 (2000).

[24] G. Dergham, D. Sipp, and J.-Ch. Robinet, Stochastic dynamics and model reduction of amplifier flows: The backward facing step flow, J. Fluid Mech. **719**, 406 (2013).

[25] S. E. Turton, L. S. Tuckerman, and D. Barkley, Prediction of frequencies in thermosolutal convection from mean flows, Phys. Rev. E **91**, 043009 (2015).

[26] S. J. Illingworth, J. P. Monty, and I. Marusic, Estimating large-scale structures in wall turbulence using linear models, J. Fluid Mech. **842**, 146 (2018).

[27] K. Sasaki, R. Vinuesa, A. V. G. Cavalieri, P. Schlatter, and D. S. Henningson, Transfer functions for flow predictions in wall-bounded turbulence, J. Fluid Mech. **864**, 708 (2019).